33 GHz Overmoded Bulk Acoustic Resonator

Zachary Schaffer, Student Member, IEEE, Pietro Simeoni, Student Member, IEEE, and Gianluca Piazza, Senior Member, IEEE

Abstract—In this work we present a new class of thickness extensional microelectromechanical resonator, overmoded bulk acoustic resonator (OBAR) for filtering applications in the 5G millimeter wave (mm-wave) spectrum. This resonator operates in a 2nd overtone thickness mode with approximately equal thickness electrodes and piezoelectric layer so that acoustic energy is distributed evenly between the different layers. Compared to a fundamental mode at a fixed frequency, the OBAR possess a 3 times thicker piezo layer and 5-10 times thicker metal electrodes, enabling manufacturable 30-60 GHz devices. We demonstrate the OBAR experimentally through fabrication of a Pt-AIN-Al device with electromechanical-coupling coefficient (k_t^2) of 1.7%, and series resonance quality factor (Os) of 110 at 33 GHz.

Index Terms—MEMS, mm-wave, 5G, aluminum nitride, piezoelectric resonators, acoustic filters.

I. INTRODUCTION

TH Generation (5G) cellular network technology addresses the growing need for high speed data transfer by operating in the millimeter wave (mm-wave) range (frequencies from 30-60 GHz). Piezoelectric resonators have been heavily commercialized for filtering in the 0.8-3 GHz range and seen adoption for sub-6 GHz bands. Direct filtering of mm-wave signals is currently only achieved through electromagnetic (EM) filters. [1] While less of an issue than for sub-6 GHz, due to relative propagation speed between EM and acoustic waves EM filters are still significantly larger than their piezoelectric counterparts. This limits how many filter elements can be used in a Radio Frequency Front-End (RFFE) due to footprint constraints. Additionally, EM filters generally have lower quality factors (Q), increasing insertion loss and causing filter distortion. Piezoelectric resonator solutions would enable novel RFFEs with direct filtering at each antenna element [2].

Scaling piezoelectric resonators to work in the 30-60 GHz frequency range presents new challenges. Thin film bulk acoustic wave resonators (FBAR) are a popular approach for sub-6 GHz filtering, and FBARs up to 24 GHz have been demonstrated as stand alone devices or in bandpass filters [3], [4]. Continuing to scale FBARs or other resonators operating in fundamental extensional modes beyond 30 GHz results in layer thicknesses that are not practical to manufacture. Additionally,

This work was supported in part by the U.S. National Science Foundation under Grants 2133388 and 1941183. Corresponding author: Z. Schaffer

Zachary Schaffer is with Carnegie Mellon University, Pittsburgh, PA 15213 USA (e-mail: zschaffer@cmu.edu)

Pietro Simeoni was with Carnegie Mellon University, Pittsburgh, PA 15213 USA. He is now with Northeastern University, Boston, MA 02115 (e-mail: p.simeoni@northeastern.edu)

electrical loading—losses from the resistance of resonator electrodes—scales extremely unfavourably with frequency for FBARs in the 30-60 GHz range reducing quality factor at series resonance (Qs) below what is needed for low loss bandpass filters. Electrical loading can be partially reduced through patterning of thick metals in inactive regions, but for the fundamental mode, metal thickness in the active region becomes prohibitive as frequency scales [5]. Other device topologies for frequency scaling have been proposed, but these rely on either very high overtones [6], or using finely patterned electrodes to excite combined modes [7], all of which have k_t^2 values limited below 2% for pure AlN.

We propose the Overmoded Bulk Acoustic Resonator (OBAR) which allows practical film thicknesses, high k_t^2 , and minimal electrical loading. The OBAR (Fig. 1) functions in a $2^{\rm nd}$ overtone thickness mode evenly split between the piezoelectric and electrode layers allowing a k_t^2 of up to 1/2 the fundamental mode with optimal electrode material (~4% for AlN). In this work we demonstrate a ~50 Ω matched Pt-AlN-Al OBAR operating at 33 GHz with 1.7% k_t^2 and series resonance $\Omega > 100$.

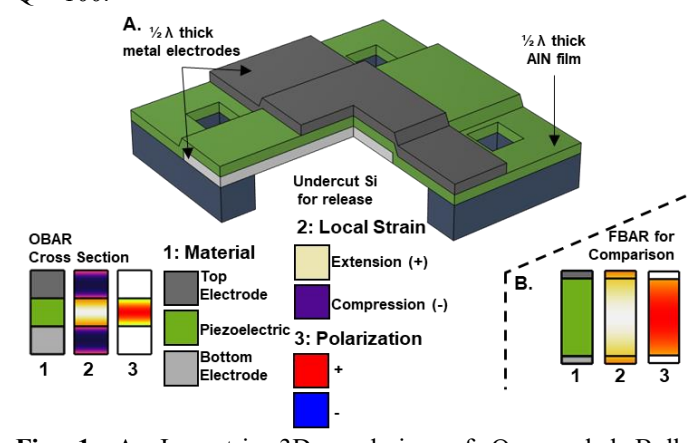


Fig. 1. A. Isometric 3D rendering of Overmoded Bulk Resonator (OBAR) with cutaway cross section views colored by 1 material, 2 local strain, 3 polarization. B. FBAR cross section views provided for comparison.

Gianluca Piazza is with Carnegie Mellon University, Pittsburgh, PA 15213 USA (e-mail: piazza@ece.cmu.edu)

Color versions of one or more of the figures in this article are available online at http://ieeexplore.ieee.org

1

II. DESIGN

A. Principle of Operation

The OBAR functions in a 2nd overtone, but instead of confining acoustic energy solely to the piezoelectric layer, the mode is split evenly between the piezoelectric layer and each electrode. The piezoelectric layer and each electrode have thicknesses equal to $\frac{1}{2}$ the acoustic wavelength (λ), leading to a mode shape within the transduced region (piezoelectric layer) similar to a fundamental mode. This prevents the typical problem of overtones in which regions of expansion and contraction produce positive and negative polarizations which cancel net charge, thereby reducing k_t^2 .

B. Frequency Scaling Analysis

As material thicknesses are scaled down, fabrication challenges related to thickness variation, trimming accuracy, and defect heavy regions near interfaces become more impactful. This is especially a problem for sputtered AlN, since its grains need to be well oriented to preserve piezoelectric properties. There is ongoing work to explore material properties of extremely thin AlN and ScAlN films [8], optimize deposition of these films [9], and demonstrate extremely thin film piezoelectric devices [10]. Since the frequency of a thickness mode is proportional to film thickness, this leads to limits in maximum manufacturable device frequency.

In devices where the metal electrodes are in the path of the acoustic wave-FBARs, OBARs, and most thickness extensional resonators—the electrode material and thickness also plays a role in setting center frequency. Adjusting the ratio of electrode to piezoelectric thickness (r_{e-p}) can improve this limit by increasing one layer thickness at the cost of the other. In Fig. 2, it is shown that at any given frequency the OBAR has a 2-3.5 times thicker piezoelectric layer and 5-10 times thicker metal electrodes than a fundamental mode device, allowing practical fabrication of devices in the 30-60 GHz range. Since electrode resistance is inversely proportional to thickness, electrical loading is also greatly reduced in OBAR structures.

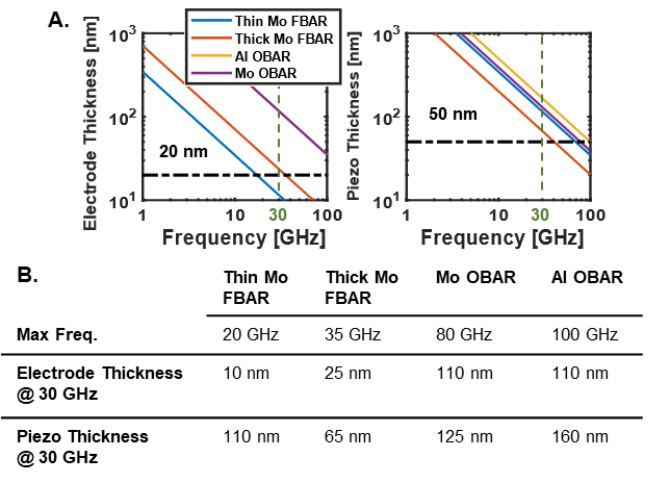


Fig. 2. A. Layer thickness vs resonant frequency for Mo-AlN-Mo fundamental mode (FBAR) and various electrode material OBAR devices. B. Maximum fabricable device frequency and layer thicknesses for a 30 GHz device.

C. Electromechanical Coupling (k_t^2) Analysis

 k_t^2 is primarily a function of the piezoelectric layer but is also impacted by electrode material and thickness. To understand this impact, it is helpful to evaluate materials based on acoustic impedance (Z) as defined in Eq. 1 based on density (ρ) and Young's modulus (E).

$$Z = \sqrt{E \cdot \rho} \tag{1}$$

 $Z = \sqrt{E \cdot \rho}$ (1) In fundamental extensional modes electrode selection has minor impact and can boost k_t^2 10-20% beyond that of the plain piezoelectric layer. [11] Primarily, this enhancement occurs from improved acoustic confinement in the piezoelectric layer from Z mismatch at the electrode interface—meaning high Z electrodes boost k_t^2 more.

Considering $\sim 2/3$ of the acoustic path length in an OBAR is electrode, material selection plays a significant role in attainable k_t^2 . An OBAR distributes acoustic energy between the piezoelectric layer and electrodes, so acoustic confinement in the piezoelectric layer is detrimental. Instead k_t^2 can be maximized by minimizing the acoustic load from the electrodes—meaning low Z electrodes are preferable. 2D Finite Element Analysis (FEA) eigenfrequency studies with grounded and free electrical boundary conditions are run to demonstrate this effect. Fig. 3 shows r_{e-p} vs k_t^2 for an Al-AlN-Al OBAR, and the max k_t^2 attainable with commonly used metals.

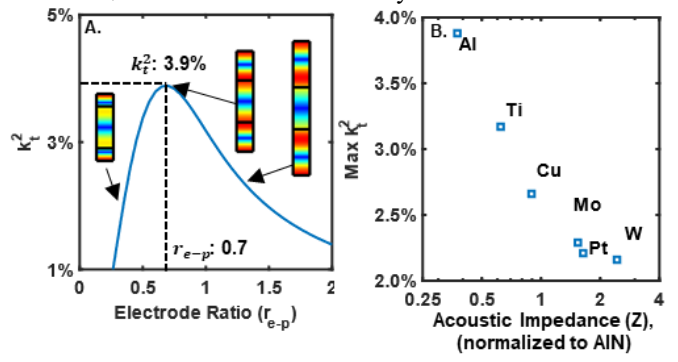


Fig. 3. A. FEA simulations of electrode ratio vs k_t^2 for Al-AlN-Al with inserts of mode shape. B. Maximum k_t^2 (k_t^2 at optimal ratio of electrode to piezoelectric layer, r_{e-p}) for commonly used metals sorted by acoustic impedance (Z)

D. Quality Factor (Q) Analysis

Q is set by a combination of intrinsic and extrinsic loss sources within a resonator. Extrinsic losses are likely dominated by anchor loss and electrical loading, which are both a function of device geometry. For intrinsic loss we expect phononphonon damping in all layers and free electron-phonon damping in the metals to dominate intrinsic losses. Phononphonon interactions change between the Akhiezer [12] and Landau-Rumer [13] regimes as λ surpasses the phonon mean free path (inversely proportional to thermal time constant of material (τ_{th})). Akhiezer regime damping is proportional to frequency, while damping in the Landau-Rumer regime is frequency independent. As frequency scales up, Q from phonon phonon damping becomes fixed. Uncertainty in the τ_{th} of these materials due to large discrepancies between bulk material and sputtered thin film thermal conductivities [14] make it unclear

MWCL-22-0239

what regime this device is in. Phonons can also interact with and scatter from charge carriers. In the case of free electrons in the metal, these scattering losses are frequency dependent and may be significant. Because of this there is likely a design tradeoff between k_i^2 and Q. Further investigation is needed to extract accurate material properties, isolate these losses, and to verify these assumed loss mechanisms.

III. EXPERIMENTAL RESULTS

A. Fabrication

The OBAR reported in this work, has lateral dimensions of 14 µm x14 µm (196 µm²) in order to be approximately 50 Ω matched. The stack consists of a 70 nm Pt bottom electrode with 10 nm Cr adhesion layer, 140 nm AlN piezoelectric layer, and 90 nm Al top electrode. While a Pt bottom electrode is suboptimal for k_t^2 , we have a tuned process for depositing very thin AlN on Pt layers. 2D FEA simulation predicts a k_t^2 of 2.1% for this stack.

A 3 mask process is used for fabrication as shown in Fig 4. In step 1) a 70 nm Pt with 10 nm Cr adhesion layer is blanket DC-sputtered onto a 4" high resistivity Si wafer to form the bottom electrode. Pattering is then done by ion milling of the Pt and Cr layers with a photoresist mask. This results in a more continuous AlN film, compared to liftoff. In step 2) AlN is deposited at low power (3 kW) using a Tegal AMS AlN sputtering tool. In step 3) the AlN is wet etched in heated CD26 (TMAH). In step 4) 90 nm of Al is DC sputtered and patterned by liftoff. Finally in step 5) the Si is undercut to release the active region using XeF₂.

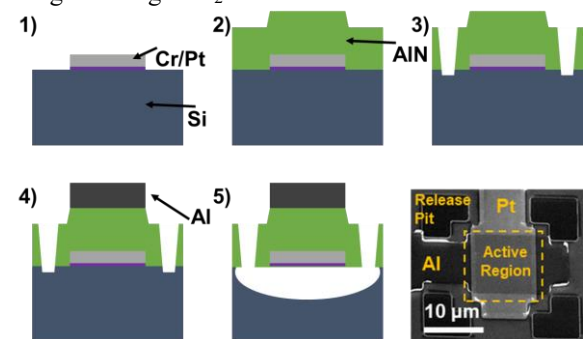


Fig. 4. OBAR process flow and SEM of fabricated device.

B. Results

The fabricated OBAR was measured on an Agilent PNA-X in a thru configuration using two 150 μ m pitch GSG probes. An initial Short Open Load Thru (SOLT) calibration was run for the probes with a cal kit, and on chip open and short structures were used to extend the reference frame from the probe tips to the edge of the device.

To extract accurate values of k_t^2 and Q, the measurement is fit to a modified Butterworth-Van Dyke (mBVD) model with series resonance Q (Qs), parallel resonance Q (Qp), and k_t^2 defined by electrical equivalent circuit relations as show in Eq. 2. An overlay of measurement and model fit is shown in Fig. 5.

$$Q_{s} = \frac{\sqrt{\frac{L_{m}}{C_{m}}}}{R_{m} + R_{s}}; \ Q_{p} = \frac{\sqrt{\frac{L_{m}}{C_{m}}}}{R_{m} + R_{0}}; k_{t}^{2} = \frac{\pi^{2} C_{m}}{8 C_{0}}$$
(2)

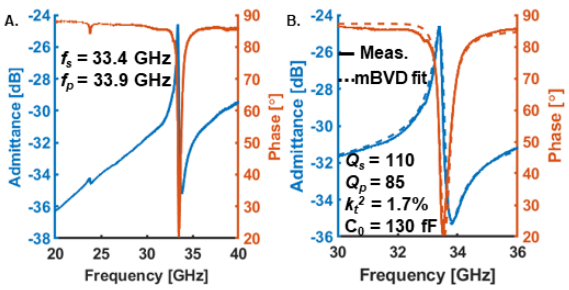


Fig. 5. A. Device admittance and phase. B. Device admittance and phase with mBVD fit near resonance.

Q vs frequency based on Bode's theorem (Q_{Bode}) is calculated as demonstrated in [15], [16]. To properly calculate Q_{Bode} the device has to be reasonably centered on a Smith chart (uniform Voltage Standing Wave Ratio (VSWR)). This is accomplished by shifting the termination impedance from 50 Ω to (32+10j) Ω . Fig. 6 shows measured device S11 before and after centering and calculated Q_{Bode} vs frequency.

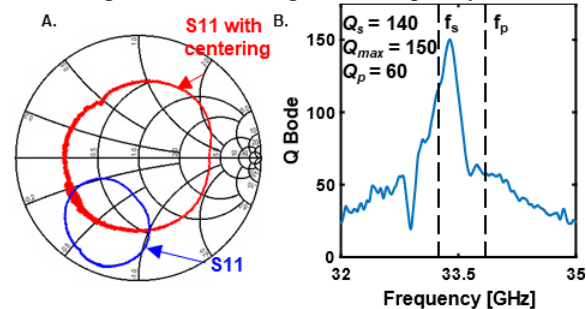


Fig. 6. A. Measured S11 with and without change in termination impedance to center response. B. Q_{Bode} vs frequency

Measured k_t^2 of 1.7% is 20% lower than FEA simulated value of 2.1% which may be due to discrepancies in material properties between the simulated and sputtered films. k_t^2 could be further improved by using a different bottom electrode material such as Mo and eliminating the Cr adhesion layer. While there is some difference in the values of Q between Q_{Bode} and the mBVD fit, both show Qs above 100 and lower Qp. This is below the Q of 290 reported by [3] for an FBAR at 24 GHz, but the electrode stack was not optimized in the current work. Losses are also currently higher than what can be accomplished with transmission line approaches implemented in CMOS fabs [1], [17], [18]. However, appropriate material selection and further optimization of the fabrication process will yield miniaturized devices with significantly improved k_t^2 (approaching 10%) and Q (> 500).

IV. CONCLUSION

In this work, we introduced the Overmoded Bulk Acoustic Resonator (OBAR) as an approach to mm-wave piezoelectric resonators. We demonstrate a ~50 Ω matched, 33 GHz Pt-AlN-Al resonator with a 140 nm thick AlN layer, 1.7% k_t^2 , and 110 Qs. We believe the combination of practical layer thicknesses and high k_t^2 make the OBAR a promising approach to scaling piezoelectric resonators to the mm-wave range.

REFERENCES

- [1] V. Narayana Rao Vanukuru and V. Krishna Velidi, "Millimeter-Wave CMOS 30/80 GHz Sharp-Rejection Dual-Band Bandstop Filters Using TFMS Open-Stepped-Impedance Resonators," *IEEE Transactions on Circuits and Systems II: Express Briefs*, vol. 68, no. 1, pp. 201–205, Jan. 2021, doi: 10.1109/TCSII.2020.3006198.
- [2] C. Fulton, M. Yeary, D. Thompson, J. Lake, and A. Mitchell, "Digital Phased Arrays: Challenges and Opportunities," *Proceedings of the IEEE*, vol. 104, no. 3, 2016, doi: 10.1109/JPROC.2015.2501804.
- [3] M. Hara, T. Yokoyama, T. Sakashita, M. Ueda, and Y. Satoh, "A study of the thin film bulk acoustic resonator filters in several ten GHz band," in *Proceedings IEEE Ultrasonics Symposium*, 2009. doi: 10.1109/ULTSYM.2009.5441576.
- [4] M. Hara *et al.*, "Super-high-frequency band filters configured with air-gap-type thin-film bulk acoustic resonators," *Japanese Journal of Applied Physics*, vol. 49, no. 7 PART 2, Jul. 2010, doi: 10.1143/JJAP.49.07HD13.
- [5] H. Park et al., "Novel Bulk acoustic wave resonator structure for reducing electrical loss of electrodes," in Proceedings - 2013 MTT-S International Microwave Symposium, 2013, doi: 10.1109/MWSYM.2013.6697524.
- [6] Y. Yang, R. Lu, T. Manzaneque, and S. Gong, "Toward Ka Band Acoustics: Lithium Niobate Asymmetrical Mode Piezoelectric MEMS Resonators," in *Proceedings - 2018 IEEE International Frequency Control Symposium*, 2018. doi: 10.1109/FCS.2018.8597475.
- [7] M. Assylbekova, G. Chen, M. Pirro, G. Michetti, and M. Rinaldi, "Aluminum Nitride Combined Overtone Resonator for Millimeter Wave 5g Applications," in *Proceedings IEEE International Conference on Micro Electro Mechanical Systems (MEMS)*, vol. 2021-January, pp. 202–205, Jan. 2021, doi: 10.1109/MEMS51782.2021.9375278.
- [8] Y. Song *et al.*, "Thermal Conductivity of Aluminum Scandium Nitride for 5G Mobile Applications and Beyond," *ACS Applied Materials & Interfaces*, vol. 13, no. 16, pp. 19031–19041, Apr. 2021, doi: 10.1021/ACSAMI.1C02912.
- [9] V. v. Felmetsger, P. N. Laptev, and R. J. Graham, "Deposition of ultrathin AlN films for high frequency electroacoustic devices," *Journal of Vacuum Science* & *Technology A: Vacuum, Surfaces, and Films*, vol. 29, no. 2, 2011, doi: 10.1116/1.3554718.
- [10] P. Simeoni and G. Piazza, "Aluminum Nitride 4-Beam Piezoelectric Nanoscale Ultrasound Transducer (pNUT)," *Journal of Microelectromechanical Systems*, 2021, doi: 10.1109/JMEMS.2021.3101461.
- [11] M. Ueda *et al.*, "Film bulk acoustic resonator using high-acoustic-impedance electrodes," *Japanese Journal of Applied Physics, Part 1: Regular Papers and Short Notes and Review Papers*, vol. 46, no. 7 B, 2007, doi: 10.1143/JJAP.46.4642.

- [12] T. O. Woodruff and H. Ehrenreich, "Absorption of Sound in Insulators," *Physical Review*, vol. 123, no. 5, p. 1553, Sep. 1961, doi: 10.1103/PhysRev.123.1553.
- [13] S. Tamura and H. J. Maris, "Spontaneous decay of TA phonons," *Physical Review B*, vol. 31, no. 4, p. 2595, Feb. 1985, doi: 10.1103/PhysRevB.31.2595.
- [14] Y. Song *et al.*, "Thermal Conductivity of Aluminum Scandium Nitride for 5G Mobile Applications and Beyond," *ACS Appl. Mater. Interfaces*, vol. 13, 2021, doi: 10.1021/acsami.1c02912.
- [15] D. A. Feld, R. Parker, R. Ruby, P. Bradley, and S. Dong, "After 60 years: A new formula for computing quality factor is warranted," in *Proceedings 2008 IEEE Ultrasonics Symposium*, pp. 431–436, 2008, doi: 10.1109/ULTSYM.2008.0105.
- [16] R. Ruby, R. Parker, and D. Feld, "Method of extracting unloaded q applied across different resonator technologies," in *Proceedings - 2008 IEEE Ultrasonics Symposium*, pp. 1815–1818, 2008, doi: 10.1109/ULTSYM.2008.0446.
- [17] D. S. Yu *et al.*, "Narrow-band band-pass filters on silicon substrates at 30 GHz," in *Proceedings IEEE MTT-S International Microwave Symposium Digest*, vol. 3, pp. 1467–1470, 2004, doi: 10.1109/MWSYM.2004.1338850.
- [18] K. T. Chan *et al.*, "40-GHz coplanar waveguide bandpass filters on silicon substrate," *IEEE Microwave and Wireless Components Letters*, vol. 12, no. 11, pp. 429–431, Nov. 2002, doi: 10.1109/LMWC.2002.805535.